

# MODELING NANOPARTICLE-STABILIZED FOAM FLOW IN POROUS MEDIA ACCOUNTING FOR PARTICLE RETENTION AND PERMEABILITY REDUCTION

Tatiana Danelon<sup>a,b</sup> , Rouhi Farajzadeh<sup>c,d</sup> , Pavel Bedrikovetsky<sup>e</sup> , Grigori Chapiro<sup>a</sup> 

<sup>a</sup>Laboratory of Applied Mathematics, Federal University of Juiz de Fora, Juiz de Fora, Brazil; <sup>b</sup>Graduate Program in Computational Modeling, Federal University of Juiz de Fora, Juiz de Fora, Brazil; <sup>c</sup>Shell Global Solutions International, Netherlands; <sup>d</sup>Department of Geoscience and Engineering, Delft University of Technology, Delft, Netherlands; <sup>e</sup>Australian School of Petroleum, Adelaide University, Adelaide, South Australia

## Correspondence to:

Tatiana Danelon,  
[tatianadanelon@gmail.com](mailto:tatianadanelon@gmail.com) or Grigori Chapiro,  
[grigori.chapiro@ufjf.br](mailto:grigori.chapiro@ufjf.br)

## How to Cite:

Danelon, T., Farajzadeh, R., Bedrikovetsky, P., & Chapiro, G. Modeling Nanoparticle-Stabilized Foam Flow in Porous Media Accounting for Particle Retention and Permeability Reduction. *InterPore Journal*, 2(1), IPJ260225–3. <https://doi.org/10.69631/ipj.v2i1nr57>

RECEIVED: 29 Nov. 2024  
ACCEPTED: 27 Jan. 2025  
PUBLISHED: 26 Feb. 2025



©2025 The Authors

## ABSTRACT

This work presents a model for nanoparticle-stabilized foam flow in porous media, accounting for particle retention and the resulting permeability reduction. We present a semi-analytical solution under steady-state conditions, which allows for obtaining water saturation, foam apparent viscosity, and pressure drop profiles. We study different nanoparticle concentrations (in the presence and absence of salt) using retention parameters based on experimental data. When particle retention is neglected, the sweep efficiency of the porous medium improves compared to the case without nanoparticles, even at a low nanoparticle concentration (0.1 wt%). In contrast, when retention is accounted for, this enhancement is observed only at higher concentrations (0.5 wt% and 1.0 wt%). Neglecting nanoparticle retention generally underestimates pressure drop, especially in scenarios with significant retention. However, while retained nanoparticles increase pressure by reducing permeability, the loss of suspended nanoparticles decreases pressure by reducing the foam's apparent viscosity. Consequently, when considering both nanoparticle loss and reduced permeability, the pressure drop is higher than in models that ignore retention. In contrast, omitting retention effects on permeability, the pressure drop is lower.

## KEYWORDS

Foam, Nanoparticles, Porous media, Particle retention

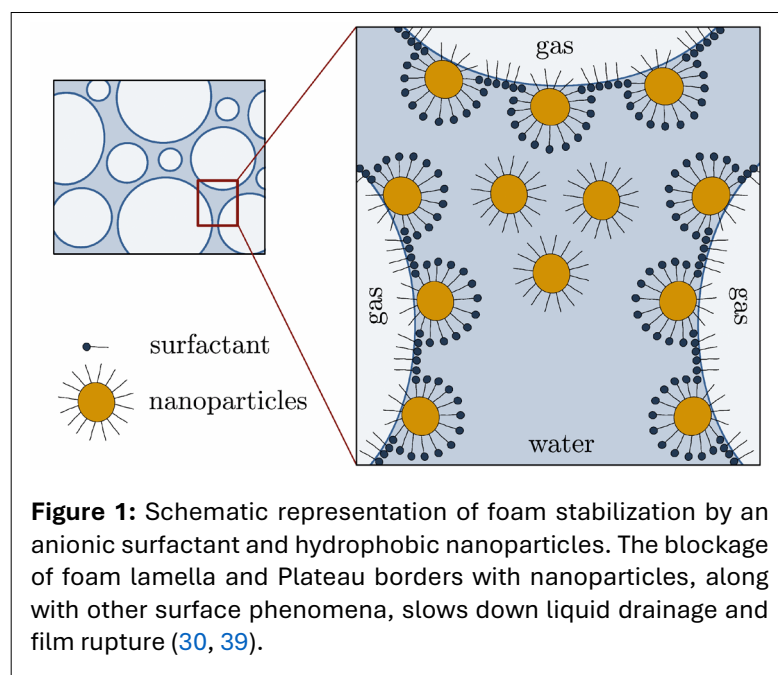
This is an open access article published by InterPore under the terms of the Creative Commons Attribution-NonCommercial-NoDerivatives 4.0 International License (CC BY-NC-ND 4.0) (<https://creativecommons.org/licenses/by-nc-nd/4.0/>).

## 1. INTRODUCTION

Nanotechnology has been rapidly growing in various industrial sectors, particularly in subsurface applications such as soil and aquifer remediation, greenhouse carbon storage, and enhanced oil recovery (EOR) (25). Nanoparticles, with a size range of 1–100 nm, can be produced with designed surface properties to meet specific demands (6). An application of nanoparticles with great potential is the stabilization of emulsions and foams, which are used as mobility-control agents to optimize gas flooding (12). The low mobility of foam helps prevent viscous fingering, channeling, and gravity override, phenomena that negatively impact the sweep efficiency of gas in porous media (14).

Due to the natural instability of foam films, maintaining long-term foam stability is a challenge. Surfactants are typically used to enhance bubble generation and resistance to coalescence, but they face limitations in field applications, where they tend to degrade faster in the presence of oil, brine, and high temperatures (32, 33). Experimental works (16, 17, 28, 34, 40, 45) have reported that adding nanoparticles improved foam stability and resistance; see (23, 46) for a detailed review. The main advantage of using solid particles as stabilizer agent lies in their high adhesion energy at the gas-liquid interface (16). Unlike surfactant molecules, nanoparticles exhibit nearly irreversible adsorption to the gas-liquid interface. This characteristic, along with the thermal and mechanical stability of nanoparticles, ensures long-term foam stability even under unfavorable conditions (12, 16, 40). A scheme of the foam stabilization process by surfactant and nanoparticles is presented in **Figure 1**.

In general, for particle injection to be effective in subsurface applications, they must meet three key criteria (47): (i) maintain stable dispersion in the injected water without forming aggregates; (ii) travel long distances with minimal retention; and (iii) attach themselves only at specific/desired locations. Particle retention is a concern as it can lead to reduced rock permeability and a decline in injectivity (i.e., increased pressure at a given flow rate) in injection wells (19). In the specific case of foam flow with suspended nanoparticles, the consequences are more complex. A high retention rate reduces the number of particles available for foam stabilization, reducing foam flow efficiency (34). Consequently, conducting a quantitative analysis of nanoparticle loss is crucial for accurately evaluating foam stability. Mechanical entrapment and adsorption are important retention mechanisms affecting the transport of particles in porous media (7, 19, 25); see **Figure 2**. Mechanical entrapment (size exclusion) occurs when pore throats block the passage of particles during a suspension flow, playing a crucial role in maintaining particle concentration over long distances (19, 36). Adsorption refers to the attachment of particles to the rock surface due to intermolecular forces, which may involve both physical and chemical interactions, affecting the propagation speed of the particle suspension in porous media (52). Pore throats in reservoir rocks are typically much larger than nanoparticles, reducing the chance of retention by size exclusion.



However, agglomeration is a significant phenomenon during nanoparticle transport and can completely alter the dominant retention mechanisms, as nanoparticle aggregates behave like larger particles (3).

Several experiments have investigated nanoparticle transport and retention in porous media (1, 11, 20, 25, 31, 35, 47, 52). The findings indicate that the main factors influencing nanoparticle retention include their type and size, the concentration and ionic strength of the injected solution,

the flow rate, and the surface charges of both nanoparticles and rock (11, 51). In (35), micromodel tests were conducted to examine the transport behavior of various types of nanoparticles ( $\text{MgO}$ ,  $\text{SiO}_2$ , and  $\text{Al}_2\text{O}_3$ ), in which high concentrations led to a significant decrease in permeability for all types, primarily due to the pore-plugging process. In (25), single-phase core-flooding experiments were performed to examine the transport of silica nanoparticles through dolomite rocks. The authors found that higher nanoparticle concentrations and increased aqueous phase ionic strength decrease nanofluid stability (the average size of nanoparticles increased), leading to greater nanoparticle retention in the rock and significant permeability reduction. Some works reported the presence or even dominance of reversible adsorption (recovery of nearly all the injected nanoparticles) during core-flooding experiments (1, 31, 47, 52). However, studies showing low nanoparticle retention often rely on an appropriate surface coating to keep the nanoparticles individually dispersed in water. In studies involving the co-injection of nanoparticle solutions (with or without surfactants) and gas, the focus is primarily on the potential of nanoparticles to stabilize foam. Notably, studies such as (33, 34, 41) included retention tests; however, these tests were conducted separately from the gas injection. It is assumed that retention is lower during foam flooding, as nanoparticles tend to migrate to the gas-liquid interface (33, 41).

Nanoparticles are expected to exhibit similar behavior to colloids (particles with diameters between 1 and 1000 nm) when they move through porous media (51). As a result, some researchers have used colloid retention models to simulate the transport of nanoparticles in saturated columns (18, 25, 29, 44, 51), allowing them to interpret experimental data. Modeling nanoparticle transport is more complicated due to the influence of various physico-chemical interactions, which can be significantly different from those affecting larger colloids. Therefore, one must be careful when extending colloid transport models to nanoparticles. A comprehensive review of crucial nanoparticle transport mechanisms and their corresponding mathematical models can be found in (3).

Although modeling foam flow in porous media is well-studied (2, 24, 26, 42, 53), incorporating nanoparticles is challenging. Two studies (13, 15) presented numerical solutions for foam models using parameters calibrated from experiments with nanoparticle-assisted foam, while another (27) introduced nanoparticle concentration as a model variable, but the solution was also limited to numerical simulations. A recent model (9) included nanoparticle transport in a foam model in local equilibrium, with the maximum foam texture depending on nanoparticle concentration. The authors obtained the global analytical solution for the system of conservation laws. A simplified version of this model was proposed in (10) to perform uncertainty quantification and sensitivity analysis studies, investigating three relevant quantities of interest: breakthrough time, cumulative water production, and pressure drop. Nevertheless, in both papers (9, 10), nanoparticles were treated as tracers in the water phase, assuming a stable colloidal dispersion without considering agglomeration or retention in the mathematical model.

In the present work, we propose a model for nanoparticle-stabilized foam flow in porous media based on the Stochastic Bubble Population (SBP) model (53). The SBP model has been experimentally validated (37, 38) and, in comparison to other foam models (24, 26), it simplifies the number of fitting parameters while remaining robust enough to predict foam behavior in porous media (53). Additionally, we have included a transport equation incorporating suspended and retained nanoparticles based on the deep-bed filtration theory (21, 36). We provide a semi-analytical solution under steady-state conditions, which is a valid approach for describing the foam-particle flow with retention for limited times (4).

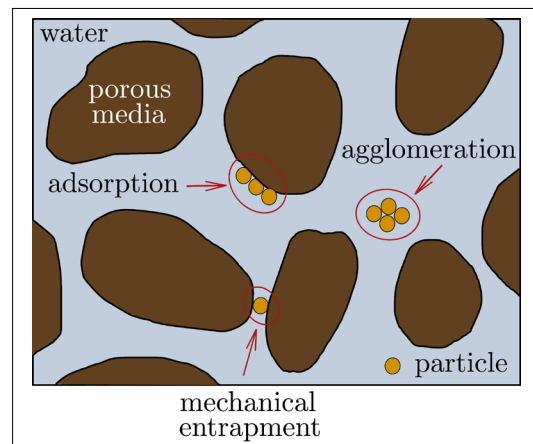


**Figure 2:** Example of processes impacting particle transport through porous media: Mechanical entrapment (size exclusion), adsorption (related to physicochemical interactions), and agglomeration (particles aggregation).

This paper is organized as follows. In [Section 2](#), we present the governing equations for nanoparticle-stabilized foam flow. The corresponding steady-state model is solved in [Section 3](#). [Section 4](#) investigates the impact of nanoparticles on foam flow through solution profiles for water saturation, foam apparent viscosity, and pressure drop. In [Section 5](#), we compare the steady-state model with a dynamic nanoparticle-stabilized foam flow model. In [Section 6](#), we discuss the results, and finally, [Section 7](#) presents the main conclusions of this work.

## 2. MATHEMATICAL MODEL FOR NANOPARTICLE-STABILIZED FOAM FLOW IN POROUS MEDIA

Following the Colloid Filtration Theory (CFT) ([21](#)), the single-phase colloidal-suspension flow is modeled by considering advection, hydrodynamic dispersion, and deposition (filtration). At low concentrations and moderate ionic strength, the single-phase flow with suspended  $C(x, t)$  and retained  $\sigma(x, t)$  particle concentration can be described by ([21](#), [43](#)) ([Eq. 1](#), [Eq. 2](#)):

$$\phi \partial_t(C + \sigma) + U \partial_x C = D \partial_{xx} C, \quad (1)$$

$$\partial_t \sigma = \lambda(\sigma)UC, \quad (2)$$

where  $U = U(t)$  is the flow velocity,  $\phi$  is the porosity,  $\lambda$  is the filtration function, and  $D$  is the hydrodynamic dispersion coefficient. Here the suspended concentration is defined as the number (volume) of particles per unit volume of the carrier fluid, while the retained concentration is defined as the number (volume) of particles per unit of the rock volume.

In many practical applications, [Equation 1](#) and [Equation 2](#) are typically analyzed at steady-state, where the effects of hydrodynamic dispersion are minimal and can be neglected ([43](#)). It is commonly assumed that the particle deposition rate remains constant over time and space ( $\lambda$  is adopted as a constant). Given these assumptions, initial conditions  $C(x, 0) = 0$ ,  $\sigma(x, 0) = 0$  and boundary condition  $C(0, t) = C^I$ , the solution of [Equation 1](#) and [Equation 2](#) is ([5](#)) ([Eq. 3](#)):

$$C(x, t) = C^I e^{-\lambda x}, \quad \sigma(x, t) = \lambda C^I (Ut - \phi x) e^{-\lambda x}, \quad (3)$$

for  $x < Ut/\phi$ ; otherwise, both concentrations  $C$  and  $\sigma$  vanish. Note that this model predicts that nanoparticle retention will continue to increase indefinitely as long as the dispersion concentration remains above zero. As a result, in a core-flooding experiment with continuous injection of dispersion, the nanoparticle effluent concentration will not reach the injection concentration (even after the breakthrough).

Different models have been proposed modifying the CFT to include other phenomena, such as detachment, agglomeration, and even adsorption (retardation); for details, see ([3](#), [50](#)). Due to the complexity of nanoparticle transport and experimental results reporting both reversible and irreversible particle capture, a mixed model including mechanical retention and adsorption seems to be the best way to model nanoparticle retention. However, there is still a lack of more rigorous studies, especially validation of mathematical models with reliable experimental data ([11](#)).

### 2.1. Model Assumptions

In this work, we study one-dimensional gas-water flow in a saturated porous medium in the presence of foam and with suspended nanoparticles in the aqueous phase. Both phases are assumed to flow during the co-injection of gas and a solution of surfactant and nanoparticles. The phases are incompressible and immiscible, and the rock is homogeneous. We also consider large-scale approximation, i.e., the diffusion terms are neglected compared with the advective fluxes.

Foam is a non-Newtonian fluid with apparent viscosity depending on the gas velocity. We include the effect of nanoparticles on foam stabilization by increasing the foam's apparent viscosity, leading to lower mobility. In addition to this positive impact, we also consider nanoparticle retention based on the CFT.

### 2.2. Governing Equations

The foam model for a gas-water flow is given by ([53](#)) ([Eqs. 4](#) and [5](#)):

$$\phi \partial_t S_w + \partial_x u_w = 0, \tag{4}$$

$$\phi \partial_t (S_f n) + \partial_x (u_f n) = \Phi, \tag{5}$$

where  $S_w$  and  $S_f$  are the water and foam/gas saturations ( $S_w + S_f = 1$ ),  $u_w$  and  $u_f$  are the water and foam superficial velocities, and  $n$  is the foam texture (the number of bubbles per unit volume).

The source term  $\Phi = \phi S_f [K_g(n_{\max} - n) - K_d n]$  depends on the bubble generation and coalescence rates ( $K_g, K_d$ ) and a reference foam texture ( $n_{\max}$ ). This term can be rewritten as  $\Phi = \phi S_f (K_d + K_g)(n_{\infty} - n)$ , where the equilibrium foam texture is  $n_{\infty} = n_{\max} K_g (K_d + K_g)^{-1}$ . Note that, mathematically, both cases  $K_d = 0$  and  $K_d \neq 0$  are equivalent (48). Thus, we consider  $K_d = 0$ , yielding  $n_{\infty} = n_{\max}$  and Equation 6:

$$\Phi = \phi S_f K_g (n_{\infty} - n) \tag{6}$$

The flow velocities  $u_w$  and  $u_f$  are determined by the extension of Darcy’s law as (8) (Eq. 7):

$$u_w = -(k k_{rw} / \mu_w) \partial_x p_w, \quad u_f = -(k k_{rf} / \mu_f) \partial_x p_f, \tag{7}$$

where  $k$  is the medium’s absolute permeability,  $k_{rj}$  is the relative permeability,  $\mu_j$  is the viscosity, and  $p_j$  is the pressure of each phase  $j = w, f$  representing the water and foam phases. We consider negligible capillary effects ( $p_w = p_f = P$ ). We assume that water can fully displace foam (the residual foam saturation is equal to zero) and foam’s relative permeability function is the same as that for free gas (Eq. 8):

$$k_{rf}(S_w) = \begin{cases} 1 - (1 - k_{rf}^0) \frac{S_w}{S_{wc}}, & 0 \leq S_w \leq S_{wc}, \\ k_{rf}^0 \left( \frac{1 - S_w}{1 - S_{wc}} \right)^{3 + \frac{2}{\beta}}, & S_{wc} < S_w \leq 1, \end{cases} \tag{8}$$

where  $S_{wc}$  is the connate water saturation,  $k_{rf}^0$  is the end-point foam relative permeability, and  $\beta$  is a constant. Analogously, the water relative permeability function is (Eq. 9):

$$k_{rw}(S_w) = \begin{cases} 0, & 0 \leq S_w \leq S_{wc}, \\ k_{rw}^0 \left( \frac{S_w - S_{wc}}{1 - S_{wc}} \right)^\beta, & S_{wc} < S_w \leq 1, \end{cases} \tag{9}$$

where  $k_{rw}^0$  is the end-point water relative permeability.

Now, let us introduce nanoparticles into Equation 4 and Equation 5. Foam is a non-Newtonian fluid with apparent viscosity given by (22) (Eq. 10):

$$\mu_f = \mu_g + \alpha(C) n u_f^{m-1}, \tag{10}$$

where  $\mu_g$  is the foam-free gas viscosity and  $m$  is a constant related to the fluid viscosity. We assume  $\alpha$  as a linear function  $\alpha(C) = \alpha_1 C + \alpha_0$  depending on the nanoparticle concentration  $C$  in the aqueous phase.

Based on the CFT (see Eq. 1 and Eq. 2) and following (7, 19) to include physicochemical adsorption, we propose the conservation law for nanoparticle transport as (Eq. 11)

$$\phi \partial_t (C S_w + a + \sigma) + \partial_x (C u_w) = 0, \tag{11}$$

where  $a$  is the concentration of nanoparticles adsorbed on the rock surface. Considering low suspension concentration, we use Henry’s (linear) adsorption isotherm, i.e.,  $a = \gamma C$ . The nanoparticle capture rate is assumed to be proportional to the dispersion-free nanoparticles flux ( $\partial_t \sigma = \lambda(\sigma) C u_w$ ), and the filtration function is constant in time and space ( $\lambda(\sigma) = \lambda$ ).

The nanoparticles retained by mechanical entrapment change the relative permeabilities of each phase, which decrease monotonically with  $\sigma$  as (5) (Eq. 12):

$$\overline{k_{rw}}(S_w, \sigma) = \frac{k_{rw}(S_w)}{(1 + \theta_w \sigma)}, \quad \overline{k_{rf}}(S_w, \sigma) = \frac{k_{rf}(S_w)}{(1 + \theta_f \sigma)}, \tag{12}$$

where  $\theta_w$  and  $\theta_f$  are positive constants called the permeability-reduction factors. Adsorption is considered low enough not to cause changes in permeability.

Consider the overall flux as the total superficial velocity of water and foam  $U(t) = u_w + u_f$ , which is independent of  $x$  due to the incompressibility of both phases. The water fractional flow function is defined as  $f_w = u_w/U$ . Following the introduction of the fractional flow theory for two-phase flow of non-Newtonian fluids (4),  $f_w$  becomes a function of the mobility ratio and the overall velocity, with (Eq. 13)

$$f_w = f_w(S_w, C, \sigma, U). \quad (13)$$

The problem is described by the following system of five unknowns ( $S_w, C, P, n$ , and  $\sigma$ ) (Eqs. 14, 15, 16, 17, 18):

$$\phi \partial_t S_w + U \partial_x f_w = 0, \quad (14)$$

$$U = -k(\overline{k_{rw}}/\mu_w + \overline{k_{rf}}/\mu_f) \partial_x P, \quad (15)$$

$$\phi \partial_t [n(1 - S_w)] + U \partial_x [n(1 - f_w)] = \phi(1 - S_w)K_g(n_\infty - n), \quad (16)$$

$$\phi \partial_t (CS_w + a + \sigma) + U \partial_x (Cf_w) = 0, \quad (17)$$

$$\partial_t \sigma = \lambda(\sigma)UCf_w. \quad (18)$$

The initial conditions corresponding to the water-saturated core with no bubbles or particles are given by (Eq. 19):

$$C = 0, \sigma = 0, n = 0, S_w = 1, \quad (19)$$

and the inlet boundary conditions corresponding to the co-injection of a chemical solution (water with surfactant and nanoparticles) and gas are (Eq. 20):

$$C = C^I, P = P^I, n = 0. \quad (20)$$

### 3. SOLVING THE NANOPARTICLE-STABILIZED FOAM STEADY STATE MODEL

The system composed of Equation 14 to Equation 18 is quite complex to allow an analytical solution. Therefore, in this section, we study the steady-state case, with the flow velocities  $u_w$  and  $u_f$  independent of  $x$ .

We divide this section into two parts. First, we investigate the foam flow model (without nanoparticles) at steady-state, presenting an analytical solution. Analogously, we study the nanoparticle-stabilized foam flow model, obtaining a semi-analytical solution.

#### 3.1. Foam flow model at steady-state

Consider normalized water saturation  $S = (S_w - S_{wc})/(1 - S_{wc})$ . At steady-state and without nanoparticles, the Darcy velocities and bubble balance equation associated with the system of Equation 14 to Equation 18 are given by (Eqs. 21, 22, 23):

$$u_w = -k \frac{k_{rw}^0}{\mu_w} S^\beta d_x P, \quad (21)$$

$$u_f = -k \frac{k_{rf}^0}{\mu_g + \alpha_0 n u_f^{m-1}} (1 - S)^{3 + \frac{2}{\beta}} d_x P, \quad (22)$$

$$d_x n = \phi u_f^{-1} (1 - S_{wc})(1 - S)K_g(n_\infty - n). \quad (23)$$

Let us consider the constant  $A = (u_w \mu_w k_{rw}^0)/(u_f k_{rf}^0)$ . The solution procedure follows four steps.

**Step 1:** Equate pressure gradient from Equation 21 and Equation 22, to obtain an expression describing the foam texture (Eq. 24):

$$n(x) = \frac{AS^{-\beta}(1-S)^{3+\frac{2}{\beta}} - \mu_g}{\alpha u_f^{m-1}}. \quad (24)$$

**Step 2:** Substitute **Equation 24** and its derivative in relation to  $x$  into **Equation 23**, to obtain an expression for  $d_x S$  (**Eq. 25**):

$$d_x S = \frac{\left[ AS^{-\beta}(1-S)^{3+\frac{2}{\beta}} - \mu_g - \alpha u_f^{m-1} n_\infty \right] (1-S) \phi K_g (1-S_{wc})}{\beta S^{-\beta-1} (1-S)^{3+\frac{2}{\beta}} + \left( 3 + \frac{2}{\beta} \right) S^{-\beta} (1-S)^{2+\frac{2}{\beta}} Au_f}. \quad (25)$$

**Step 3:** Assuming that there is no bubble at the inlet ( $n(0) = 0$ ), from **Equation 24** we obtain (**Eq. 26**):

$$S^{-\beta} (1-S)^{3+\frac{2}{\beta}} - \mu_g / A = 0. \quad (26)$$

This is the transcendental equation for  $S(x=0) = S^I$ , allowing us to determine the inlet boundary condition for water saturation.

**Step 4:** Distribution  $n(x)$  is calculated by **Equation 24** for known profile  $S(x)$ . The pressure profile is obtained by (**Eq. 27**):

$$P(x) = P^I - \frac{u_w \mu_w}{k k_{rw}^0} \int_0^x S(x)^{-\beta} dx. \quad (27)$$

Note that the solution  $S(x)$  can be obtained by separation of variables (**Eq. 28**), where the function  $g(S)$  is defined as the right side of **Equation 25**.

$$\int_{S^I}^{S(x)} \frac{1}{g(S)} dS = x, \quad (28)$$

### 3.2. Foam flow model with nanoparticles at steady-state

Consider normalized water saturation  $S = (S_w - S_{wc}) / (1 - S_{wc})$ . At steady-state, the Darcy velocities and bubble balance equation associated with the system of **Equations 14 to 18** are given by (**Eqs. 29, 30, and 31**):

$$u_w = - \frac{k k_{rw}^0 S^\beta}{\mu_w (1 + \theta_w \sigma)} d_x P, \quad (29)$$

$$u_f = - \frac{k k_{rf}^0 (1-S)^{3+\frac{2}{\beta}}}{[\mu_g + (\alpha_1 C + \alpha_0) n u_f^{m-1}] (1 + \theta_f \sigma)} d_x P, \quad (30)$$

$$d_x n = \phi u_f^{-1} (1 - S_{wc}) (1 - S) K_g (n_\infty - n). \quad (31)$$

Since adsorption only delays the front propagation of the nanoparticle, it will have no impact on this steady-state analysis.

According to the CFT, the solution for  $C$  and  $\sigma$  is given by **Equation 3**; see (5) for details. As we are looking for the stationary solution, using a constant  $\Gamma$ , we approximate the retained nanoparticle concentration as (**Eq. 32**):

$$\sigma(x) = \Gamma C(x) = \Gamma C^I e^{-\lambda x}, \quad (32)$$

which is valid for a limited time. Since  $C$  varies along the core, we still consider mechanical entrapment, with the retained concentration changing with  $x$ .

Analogous to the previous case (**Subsection 3.1**), the solution procedure follows four steps.

**Step 1:** Equate pressure gradient from **Equation 29** and **Equation 30**, to obtain an expression describing the foam texture (**Eq. 33**) where  $A = (u_w \mu_w k_{rw}^0) / (u_f k_{rf}^0)$ .

$$n(x) = \frac{A \left( \frac{1 + \theta_w \Gamma C^I e^{-\lambda x}}{1 + \theta_f \Gamma C^I e^{-\lambda x}} \right) (1 - S)^{3 + \frac{2}{\beta}} S^{-\beta} - \mu_g}{(\alpha_1 C^I e^{-\lambda x} + \alpha_0) u_f^{m-1}}, \quad (33)$$

**Step 2:** Substitute **Equation 33** and its derivative in relation to  $x$  into **Equation 31**, to obtain an expression for  $d_x S$  (**Eq. 34**):

$$\begin{aligned} d_x S = & - \left[ \frac{\alpha_1 C^I e^{-\lambda x} + \alpha_0}{u_f^{1-m}} \left( \frac{\alpha_1 C^I \lambda u_f^{1-m} e^{-\lambda x} (\mu_g - AB(1 - S))}{(\alpha_1 C^I e^{-\lambda x} + \alpha_0)^2} \right. \right. \\ & - \left. \frac{\phi K_g (1 - S_{wc})(S - 1)}{u_f} \left( n_\infty + \frac{u_f^{1-m} (\mu_g - AB(1 - S))}{\alpha_1 C^I e^{-\lambda x} + \alpha_0} \right) \right) \\ & + \left. \frac{AB(1 - S) \lambda e^{\lambda x} \Gamma (\theta_f - \theta_w) C^I}{(e^{\lambda x} + \Gamma \theta_w C^I)(e^{\lambda x} + \Gamma \theta_f C^I)} \right] \cdot \left[ AB \left( \frac{1 - S}{S} \beta + 3 + \frac{2}{\beta} \right) \right]^{-1}, \end{aligned} \quad (34)$$

where (**Eq. 35**):

$$B = B(x, S(x)) = \frac{(1 - S)^{2 + \frac{2}{\beta}} (e^{\lambda x} + \Gamma \theta_w C^I)}{S^\beta (e^{\lambda x} + \Gamma \theta_f C^I)}. \quad (35)$$

**Step 3:** Assuming that there is no bubble at the inlet ( $n(0) = 0$ ), from **Equation 33** we obtain **Equation 36**:

$$(1 - S)^{3 + \frac{2}{\beta}} S^{-\beta} - \frac{\mu_g}{A} \left( \frac{1 + \theta_f \Gamma C^I}{1 + \theta_w \Gamma C^I} \right) = 0, \quad (36)$$

allowing us to determine the inlet boundary condition  $S(x = 0) = S^I$  for water saturation.

**Step 4:** Distribution  $n(x)$  is calculated by **Equation 33** for known profile  $S(x)$ . The pressure profile is obtained by **Equation 37**:

$$P(x) = P^I - \frac{u_w \mu_w}{k k_{rw}^0} \int_0^x (1 + \theta_w \Gamma C) S^{-\beta} dx. \quad (37)$$

Note that the right side of **Equation 34** depends on  $x$ , so the solution  $S(x)$  cannot be obtained by separation of variables as in the previous case. Therefore, we find the saturation profile numerically.

## 4. IMPACT OF NANOPARTICLES ON FOAM FLOW

This section presents the results obtained by using the steady-state solution developed in **Section 3**. We use the ODE45 solver from MATLAB to obtain the numerical water saturation profiles. Given the absence of comprehensive experimental data for nanoparticle-stabilized foam flow that would allow us to fit both the SBP and the nanoparticle retention model, we use different data for each part. Model calibration is detailed below.

### 4.1. Model calibration

The physical parameters used to calibrate the SBP model were sourced from (37), where a core-flooding experiment was conducted to study nitrogen-foam flow in natural sandstone without oil. As for the parameters related to the effect of nanoparticles on foam flow, we follow (9). In this work, the foam is in local equilibrium and changes with silica nanoparticle concentration based on literature experimental data as  $n_{max}(C) = 2531.80C + 802.58 \text{ mm}^{-3}$  (for  $0 \leq C \leq 1$  representing nanoparticle concentration between 0.0 and 1.0 wt% of the total aqueous phase). Here, we consider a bubble population balance model, so the foam texture varies along the core even at steady-state conditions. Therefore, we adjust

**Table 1:** Model parameters used in this work (9, 37).

Symbol	Parameter	Value
$\alpha_0$ (Pa·s <sup>2/3</sup> m <sup>10/3</sup> )	Viscosity proportionality const.	$5.8 \cdot 10^{-16}$
$\alpha_1$ (Pa·s <sup>2/3</sup> m <sup>10/3</sup> )	Viscosity proportionality const.	$1.83 \cdot 10^{-15}$
$\phi$ (–)	Porosity	0.21
$k$ (m <sup>2</sup> )	Absolute permeability	$2.5 \cdot 10^{-12}$
$\beta$ (–)	Pore-size-distribution parameter	5.0
$\mu_g$ (Pa·s)	Gas viscosity	$1.8 \cdot 10^{-5}$
$\mu_w$ (Pa·s)	Water viscosity	$1.0 \cdot 10^{-3}$
$m$ (–)	Power law viscosity exponent	2/3
$k_{rf}^0$ (–)	Gas endpoint relative perm.	1.0
$k_{rw}^0$ (–)	Water endpoint relative perm.	0.75
$u_w$ (m/s)	Water velocity	$1.45 \cdot 10^{-6}$
$u_f$ (m/s)	Gas velocity	$1.47 \cdot 10^{-5}$
$S_{wc}$ (–)	Connate water saturation	0.10
$S_{gr}$ (–)	Residual gas saturation	0
$K_g$ (s <sup>-1</sup> )	Bubble generation rate	0.1
$n_\infty$ (mm <sup>-3</sup> )	Equilibrium foam texture	802.58
$L$ (m)	Core length	0.17
$D$ (m)	Core diameter	0.038

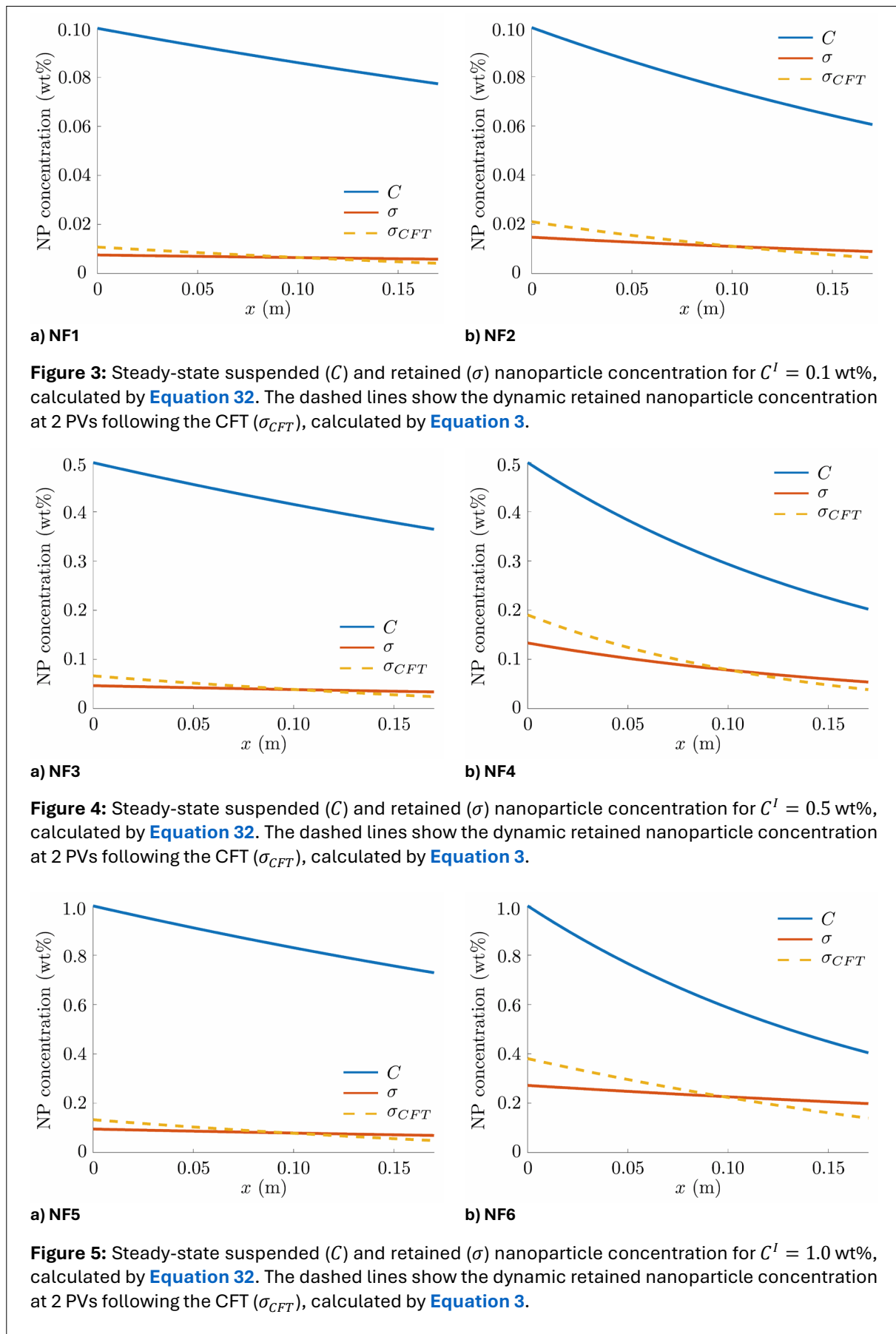
the models through the foam apparent viscosity, adopting  $n_\infty = 802.58 \text{ mm}^{-3}$ ,  $\alpha_0 = 5.8 \cdot 10^{-16} \text{ Pa s}^{2/3} \text{ m}^{10/3}$ , and  $\alpha_1 = (2531.80\alpha_0)/n_\infty \text{ Pa s}^{2/3} \text{ m}^{10/3}$ . **Table 1** summarizes the model parameters.

To calibrate the nanoparticle retention model, we follow (25), where a core-flooding experiment was conducted to investigate the transport of silica nanoparticles in dolomite rocks. The experiments were carried out on several core samples with a diameter of 3.8 cm, an average length of 10 cm, and absolute permeability ranging from 23 to 40 mD. Nanofluids with 0.1 and 0.5 wt% SiO<sub>2</sub> nanoparticle concentrations were tested with different ionic strengths and ion types (NaCl, MgCl<sub>2</sub>). The experiment was analyzed using deep-bed filtration theory, yielding the filtration ( $\lambda$ ) and the permeability-reduction ( $\theta_w$ ) coefficients under these varying conditions. In the present study, we only consider the variations in nanoparticle (NP) and salt concentrations, as shown in **Table 2**. We included two artificial nanofluids with  $C^I = 1.0\%$  wt% (NF5 and NF6). Since this nanoparticle concentration was not experimentally investigated in (25), we use the same values of  $\lambda$  and  $\theta_w$  obtained for  $C^I = 0.5\%$  wt%. This assumption may slightly overestimate or underestimate the positive effect of nanoparticles on foam flow, as increasing concentration raises foam viscosity without altering retention-related parameters. Additional experimental data is needed for more accurate estimates.

Note that the permeability-reduction factor  $\theta_w$  was obtained for a single-phase model in (25). In two-phase models involving the injection of an aqueous solution with suspended particles into an oil reservoir, permeability reduction is typically considered only for the aqueous phase. However, in this study, we examine the co-injection (or alternate injection) of gas and an aqueous solution with surfactant

**Table 2:** Nanoparticle retention parameters used in this work (25).

Nanofluid	SiO <sub>2</sub> (wt%)	NaCl (ppm)	$\lambda$ (m <sup>-1</sup> )	$\theta_w$ (–)
NF1	0.1	0	1.51	2013
NF2	0.1	50000	2.95	3269
NF3	0.5	0	1.86	1312
NF4	0.5	50000	5.33	913
NF5	1.0	0	1.86	1312
NF6	1.0	50000	5.33	913



and nanoparticles. In this scenario, the retained particles influence the relative permeability of both phases. To be more realistic, we assume that this impact varies between phases, with  $\theta_f = 0.5\theta_w$  as the equivalent parameter for gas relative permeability. This hypothesis is based on the fact that the presence of non-wetting fluids leads to lower permeability reduction due to particle retention, as there is incomplete accessibility of the available surface and pores to particles transported by the water phase (49).

Additionally, we consider  $\Gamma = 0.3\lambda$  to calculate the retained nanoparticle concentration. This value was chosen to align the simplified (steady-state)  $\sigma$  solution proposed by Equation 32 with the classical (dynamic) CFT solution calculated by Equation 3 at two injected pore volumes (PV); see Figure 3, 4, and 5. Note that, in the absence of NaCl (NF1, NF3, and NF5), the decay in the suspended and retained concentration profiles is similar for all nanoparticle concentrations. However, with NaCl (NF2, NF4, and NF6), the decay becomes more pronounced as nanoparticle concentration increases.

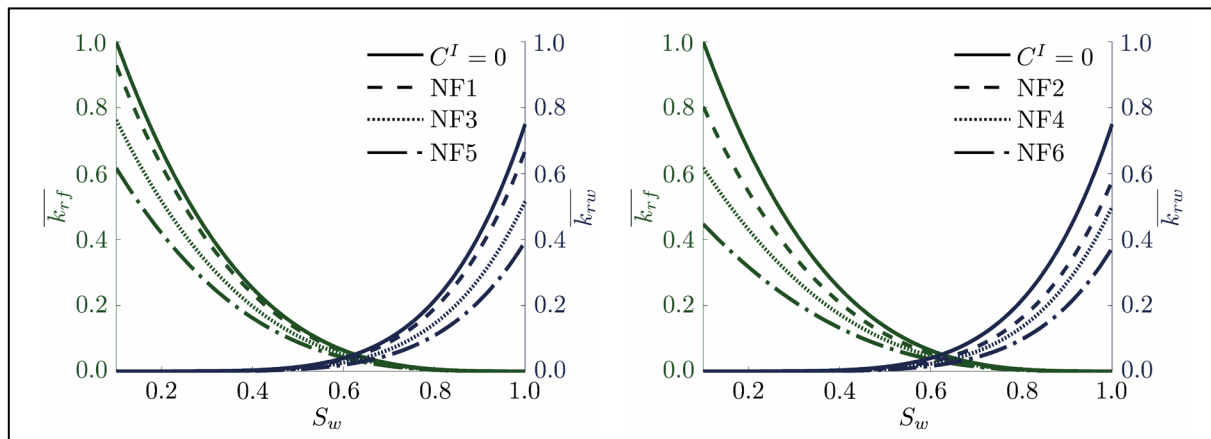
The co-injection of the nanofluid and gas can lead to nanoparticle entrapment on the rock surface and in pores accessible to both aqueous and gaseous phases, thereby reducing the relative permeabilities of water and gas. By calculating  $\overline{k_{rw}}$  and  $\overline{k_{rf}}$  using Equation 12, we obtain the curves presented in Figure 6 for nanofluids without NaCl (NF1, NF3, and NF5) and with NaCl (NF2, NF4, and NF6). This figure also displays the original curves with no particle retention (equivalent to water injection without nanoparticles, i.e.,  $C^I = 0$ ). Note that, for both cases without and with NaCl, the water permeability-reduction coefficients decrease (or remain the same) as the injected nanoparticle concentration increases; see Table 2. Even so, the endpoints of  $\overline{k_{rw}}(S_w, \sigma)$  and  $\overline{k_{rf}}(S_w, \sigma)$  decrease with increasing  $C^I$ . This occurs because  $\sigma$  varies with  $C^I$  and  $\lambda$ . In addition, the presence of salt increases particle retention (see Figs. 3, 4, and 5), resulting in a greater reduction in gas relative permeability compared to the case without salt. That is, the endpoints of  $\overline{k_{rf}}$  for NF2, NF4, and NF6 are much lower than for NF1, NF3, and NF5. As for the water relative permeability, the presence of salt is only significant for the lowest nanoparticle concentration (the endpoint of  $\overline{k_{rw}}$  for NF2 is notably lower than for NF1).

## 4.2. Nanoparticle-stabilized foam flow

The semi-analytical solution for nanoparticle-stabilized foam flow at steady-state, developed in Subsection 3.2, allows us to obtain the water saturation, apparent viscosity, and pressure drop profiles for each nanofluid. To compare these results with foam flow (without nanoparticles), we use the steady-state analytical solution developed in Subsection 3.1.

Before presenting the results for nanofluids 1-6, let us examine the effect of nanoparticles on foam flow while neglecting particle retention (i.e.,  $\lambda = 0$ ). Figure 7 shows the solution profiles. In panel (c) of Figure 7,  $P_L = P(L)$  is the pressure at the core's end. Therefore,  $P(x) - P_L$  corresponds to the pressure drop profile, while  $\Delta P = P(0) - P_L$  denotes the total pressure drop, as shown in panel (d) for each nanofluid. The addition of nanoparticles increases the foam's apparent viscosity, resulting in a reduction in water saturation along the core and an increase in pressure drop. Moreover, this effect becomes more pronounced as the concentration of injected nanoparticles increases. Lower steady-state water saturation represents better sweeping efficiency since more water has been swept from the porous medium.

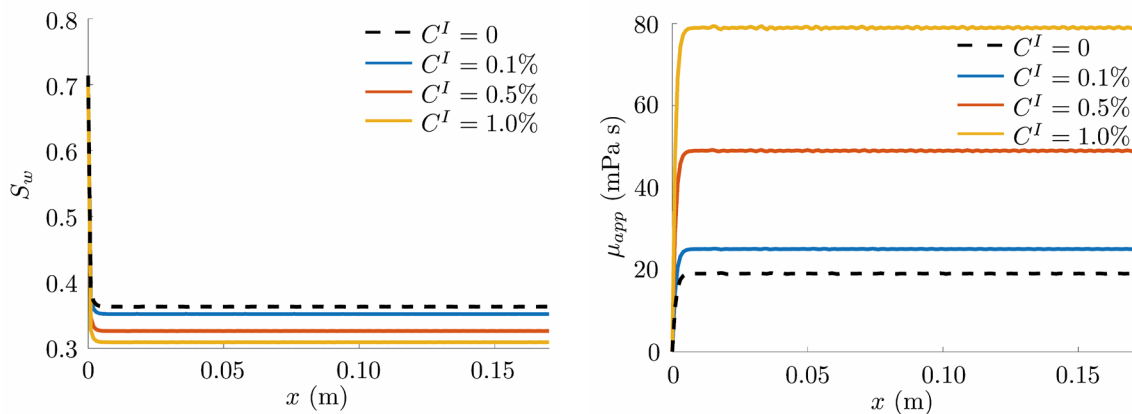
Now, let us analyze the complete model, taking into account particle retention for the case without NaCl (NF1, NF3, and NF5); see Figure 8. From the saturation profiles, we observe that the water saturation along the core is slightly higher (for all nanofluids) compared to the case without retention. Additionally, there is a decay in the foam's apparent viscosity profiles, which intensifies as the core's end is approached. These two results are associated with the loss of nanoparticles due to retention, which reduces their effect on the foam's apparent viscosity and, consequently, reduces the sweep efficiency compared to the case without retention. On the other hand, the pressure drop shows a significant increase, which aligns with the reduction in relative permeabilities caused by the retained particles. For the case with NaCl (NF2, NF4, and NF6), the results are similar; see Figure 9. However, as this case represents high ionic strength, nanoparticle retention is higher, leading to a more significant reduction in sweep efficiency and a more pronounced increase in pressure drop.



a) Nanofluids without NcCl.

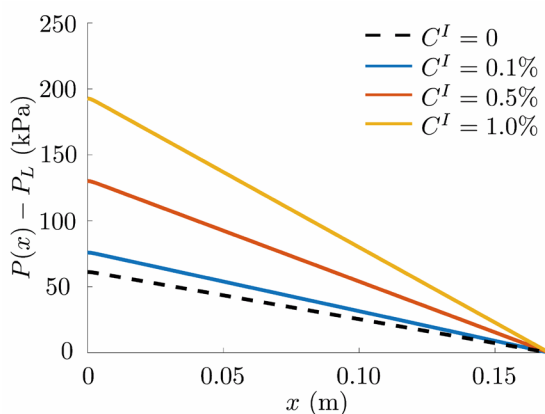
b) Nanofluids with NcCl.

**Figure 6:** Relative permeability for water ( $\overline{k_{rw}}$ , blue curves) and gas ( $\overline{k_{rg}}$ , green curves) after nanoparticle injection. The solid lines represent the original relative permeabilities (without nanoparticles retention). See Table 2 for the description of each nanofluid.



a) Water saturation.

b) Foam apparent viscosity.



c) Pressure drop.

Nanofluid	$\Delta P$ (kPa)
$C^I = 0$	61.18
$C^I = 0.1\%$	75.89
$C^I = 0.5\%$	130.20
$C^I = 1.0\%$	192.77

d) Total pressure drop.

**Figure 7:** Steady-state solution profiles for foam flow (without nanoparticles,  $C^I = 0$ ) and nanoparticle-stabilized foam flow ( $C^I = 0.1, 0.5,$  and  $1.0$  wt%) neglecting particle retention ( $\lambda = 0$ ). In panel (c),  $P(x) - P_L$  corresponds to the pressure drop profile, while  $\Delta P = P(0) - P_L$  denotes the total pressure drop shown in panel (d).

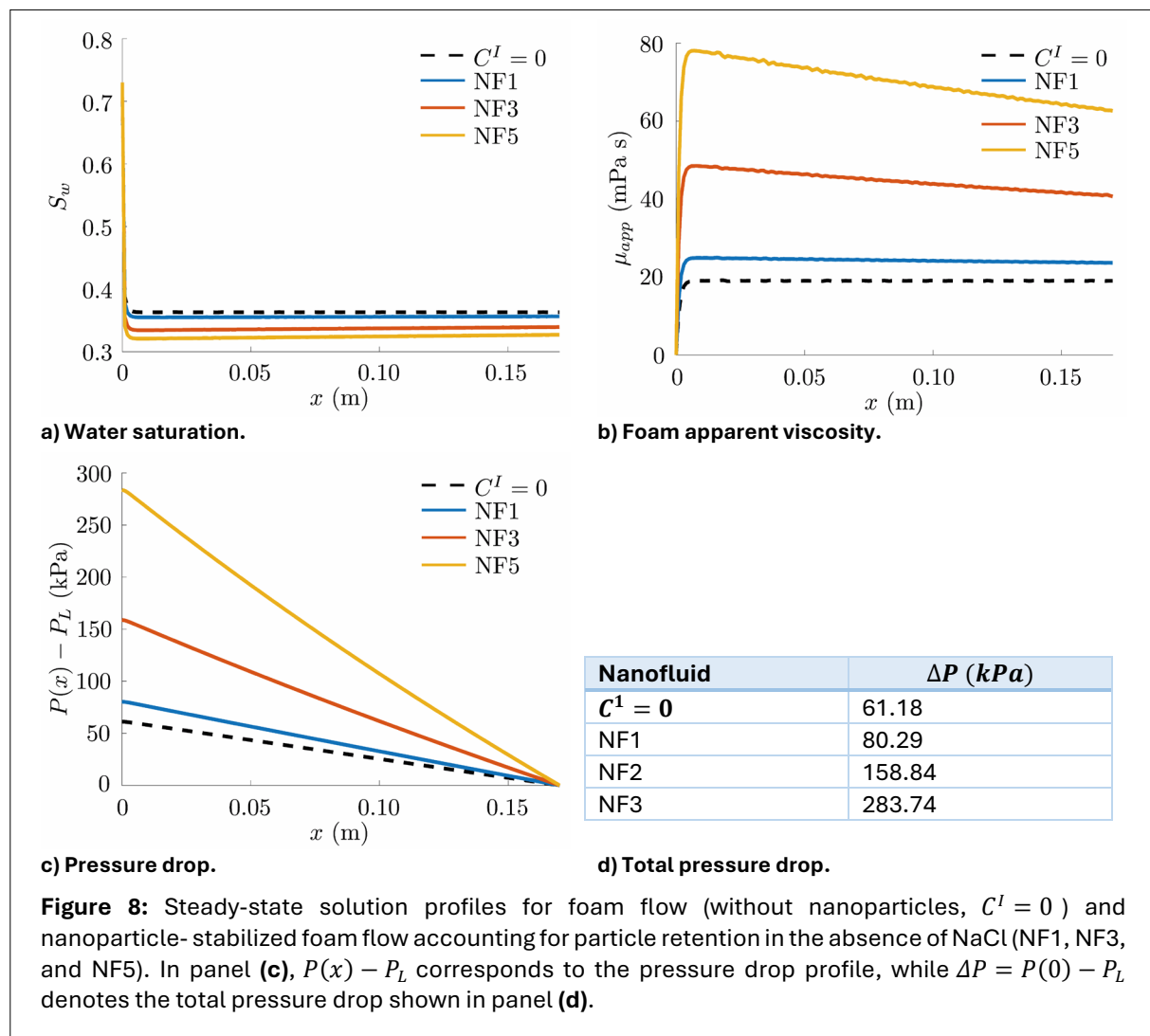


**Figure 8:** Steady-state solution profiles for foam flow (without nanoparticles,  $C^I = 0$ ) and nanoparticle-stabilized foam flow accounting for particle retention in the absence of NaCl (NF1, NF3, and NF5). In panel (c),  $P(x) - P_L$  corresponds to the pressure drop profile, while  $\Delta P = P(0) - P_L$  denotes the total pressure drop shown in panel (d).

**Remark - Section 4.1:** Note that nanoparticle loss due to retention has a clear negative impact on foam flow, as it diminishes the positive effect of nanoparticles in increasing the foam's apparent viscosity. Conversely, analyzing the impact of the resulting permeability reduction is more complex. This reduction can lead to positive outcomes, such as reducing channeling (preferential paths), as well as negative consequences, such as a decline in injectivity. Opposite effects of permeability reduction can also be observed in the pressure drop, as detailed in Section 6 ahead.

**Remark - Section 4.2:** In both laboratory and field tests, as the foam's apparent viscosity increases, higher injection rates are required to maintain efficient foam flow. However, equipment capacity and rock resistance impose a limit on the injection pressure. Thus, although the high-viscosity nature of foam solutions enhances reservoir sweep efficiency by controlling gas mobility, it reduces injectivity and can even make flow impossible. In this work, we do not establish an injection pressure limit or study injectivity decline. The nanoparticle-stabilized foam injection study presented here involves high pressure drop values (see item (c) of Figs. 7, 8, and 9), which would be impractical for field applications; however, these pressure values are compatible with laboratory experiments.

## 5. COMPARING STEADY-STATE AND DYNAMIC NANOPARTICLE-ASSISTED FOAM FLOW MODELS

Let us compare the steady-state model introduced in Section 3 with a dynamic nanoparticle-assisted foam flow model (9). Using definitions analogous to what was presented in Section 2, in (9) the following system is investigated (Eq. 38, Eq. 39):

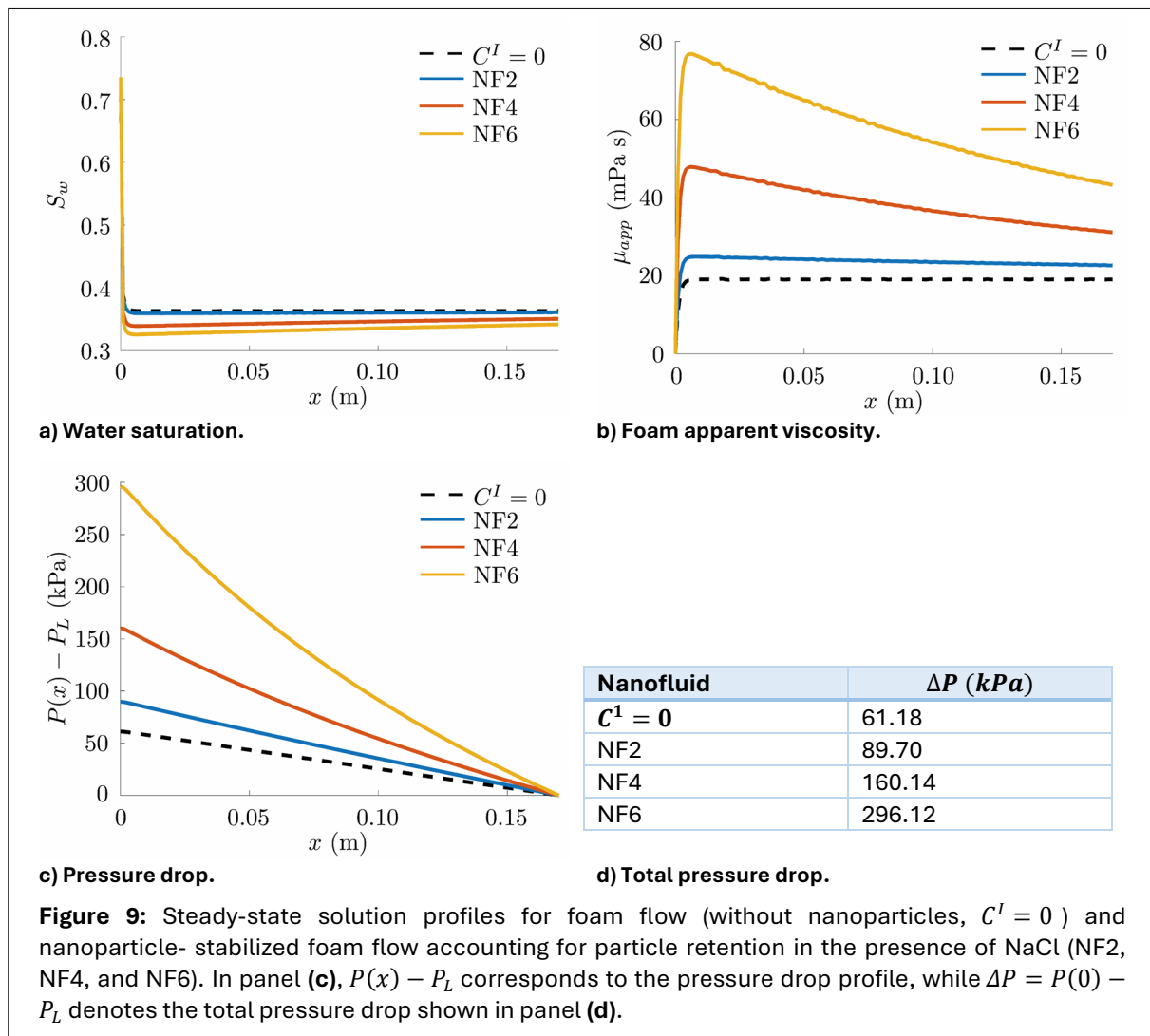


**Figure 9:** Steady-state solution profiles for foam flow (without nanoparticles,  $C^I = 0$ ) and nanoparticle- stabilized foam flow accounting for particle retention in the presence of NaCl (NF2, NF4, and NF6). In panel (c),  $P(x) - P_L$  corresponds to the pressure drop profile, while  $\Delta P = P(0) - P_L$  denotes the total pressure drop shown in panel (d).

$$\phi \partial_t S_w + U \partial_x f_w = 0, \tag{38}$$

$$\phi \partial_t (C S_w) + U \partial_x (C f_w) = 0. \tag{39}$$

Foam is in local equilibrium and its effect was included by reducing the gaseous phase mobility as  $k_{rf}(S_w, C) = k_{rg}^0(S_w) / (\mathcal{B} n_{max}(C) + 1)$ , where  $k_{rg}^0$  is the end-point gas foam-free relative permeability and  $\mathcal{B}$  is a mobility parameter defined as  $\mathcal{B} = \alpha_0 / (u_f^{m-1} \mu_g)$ . The equilibrium foam texture  $n_{max}(C)$  changes with nanoparticle concentration.

In (9), the authors investigated the existence of a global solution of the system of Equation 38 and Equation 39 as a sequence of waves following the Conservation Laws Theory, classifying the phase-plane  $S_w - C$  according to six solution types. Nevertheless, particle retention was not included in this model. To appropriately compare the results, we analyze Equation 29 to Equation 31 without retention ( $\lambda = 0$ ), which yields a specific case of the solution developed in Subsection 3.2 for the complete system. In addition, we consider the dynamic model solution for large times after all waves have reached the core's end.

In this section, we will refer to the model proposed in this paper as the PB (population balance) model and the one proposed in (9) as the LE (local equilibrium) model. For the PB model, the initial and boundary conditions are described by Equation 19 and Equation 20. For the LE model, in which we have only two unknowns ( $S_w$  and  $C$ ), we also consider the core to be initially saturated with no particles ( $S_w(x, 0) = 1, C(x, 0) = 0$ ) and with the same injected nanoparticle concentration ( $C(0, t) = C^I$ ). However, the injected water saturation  $S_w^I$  is chosen as the saturation at the core outlet obtained by the PB model rather than being set as a boundary condition.

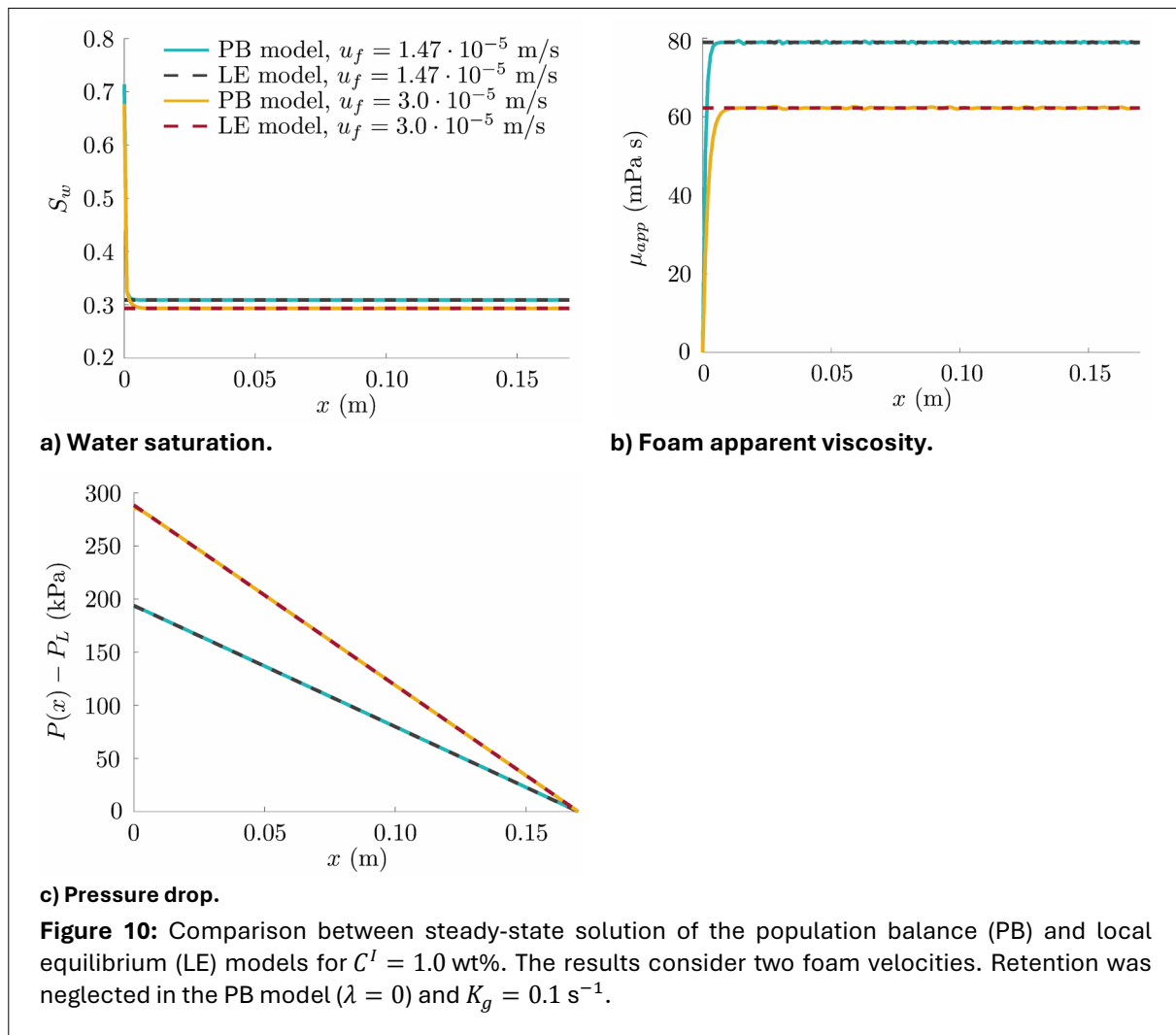
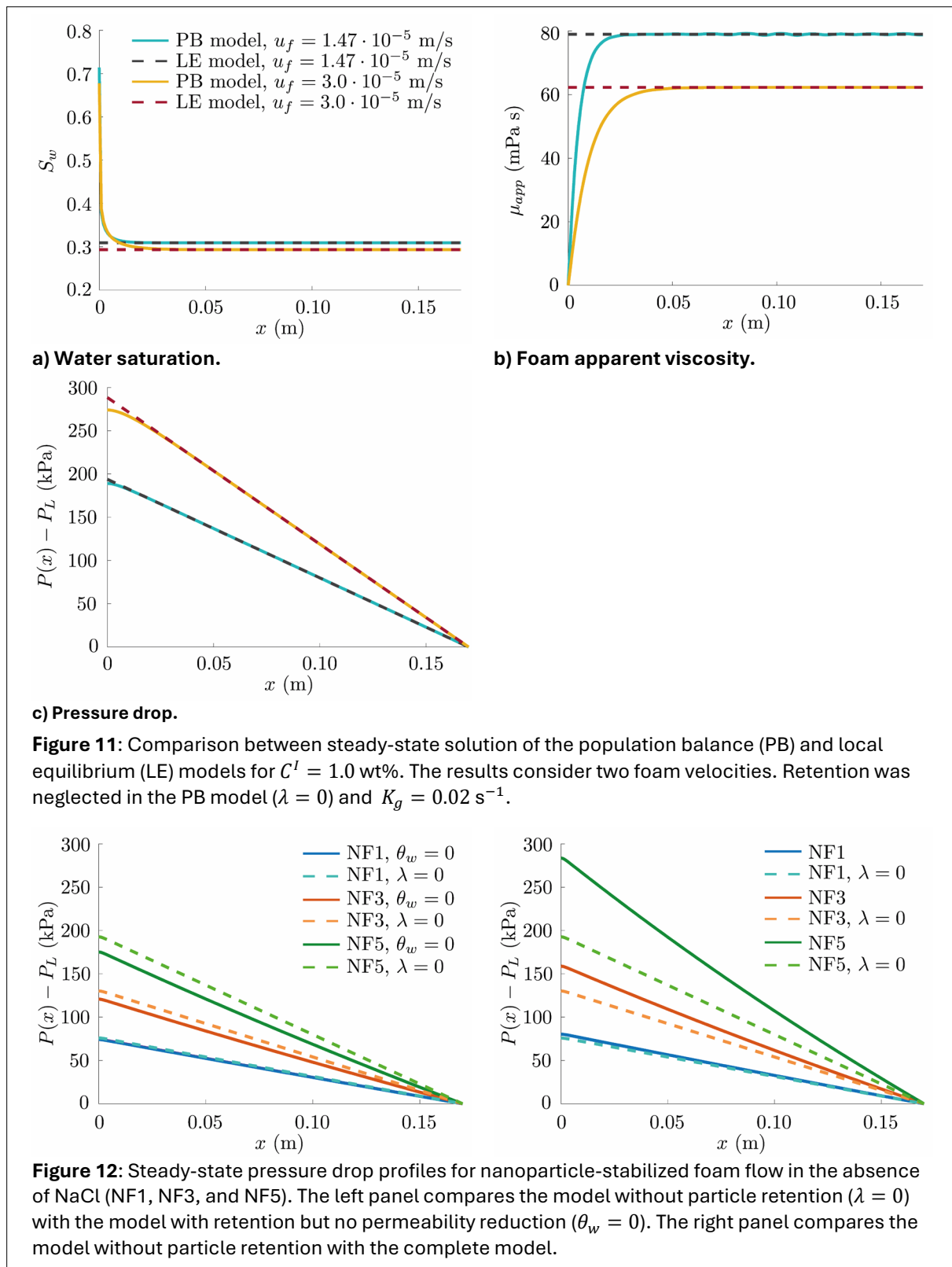


**Figure 10** compares each model's water saturation, foam apparent viscosity, and pressure drop profiles at steady-state for  $C^I = 1.0$  wt%. The blue and gray lines show results obtained with the same fluid velocities presented in **Table 1** ( $u_w = 1.45 \cdot 10^{-6} \text{ m/s}$  and  $u_f = 1.47 \cdot 10^{-5}$ ), while the red and yellow lines represent results for a higher gas velocity ( $u_f = 3.0 \cdot 10^{-5} \text{ m/s}$ ). There is a good agreement between the results, even considering no bubbles at  $x = 0$  in the PB model. That is, foam is generated very close to the core's inlet, and the bubble density can be well approximated by an equilibrium value  $n_\infty$ . It is also possible to observe changes in the solution according to the foam velocity due to the non-Newtonian behavior of the foam.

To obtain the results of **Figure 10**, we considered a high bubble generation rate ( $K_g = 0.1 \text{ s}^{-1}$ ). **Figure 11** shows the solution for a lower value ( $K_g = 0.02 \text{ s}^{-1}$ ). In this case, the LE model does not describe the foam behavior as well at the core's inlet, since the foam is generated further along the core.

## 6. Summary and Discussion

We proposed a new model for nanoparticle-stabilized foam flow in porous media, considering retention and the resulting permeability reduction. Analyzing the steady-state simplification of the model, we derived an analytical solution for the foam flow without nanoparticles and a semi-analytical solution for the complete case of foam assisted by nanoparticles. In this section, we examine our results in greater detail; we discuss further research to enhance the understanding of nanoparticle-stabilized foam flow.



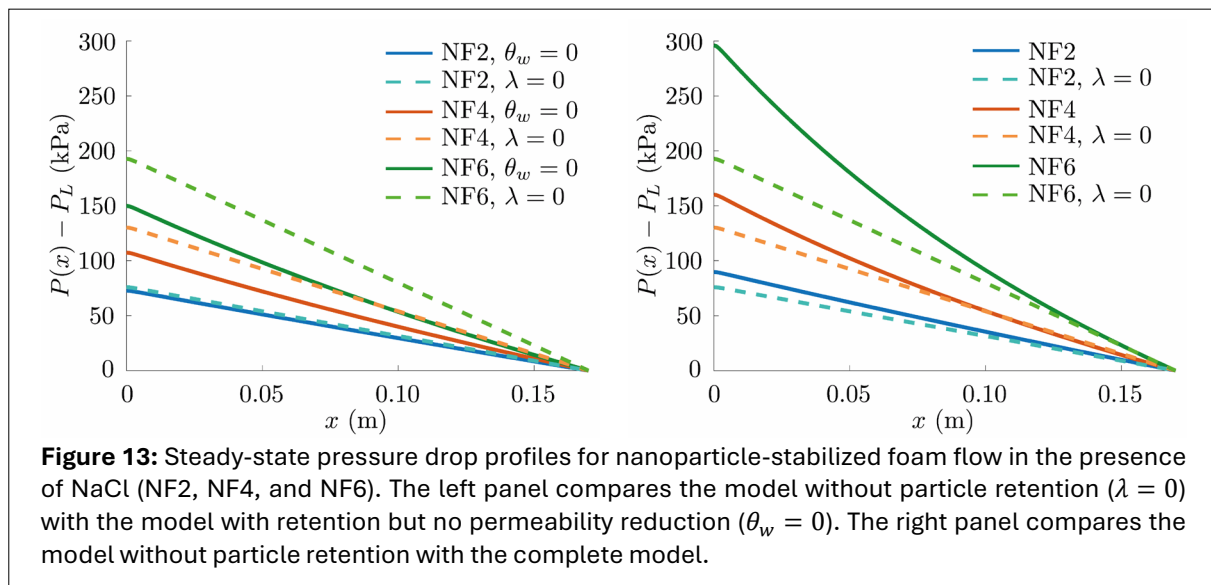
As shown in Section 4, when particle retention is neglected, nanoparticles improve the sweep efficiency of the porous medium by increasing foam apparent viscosity. This results in a lower steady-state water saturation and a higher pressure drop. However, when nanoparticle retention is considered, two effects occur: (i) the loss of suspended nanoparticles reduces their impact on  $\mu_{app}$ , and (ii) the retained nanoparticles reduce the relative permeabilities. Mathematically, both effects lead to an increase in water saturation, which generally decreases the pressure drop compared to a model that neglects retention. Nevertheless, the reduction in permeability directly increases the pressure drop (see Eq. 37). As a result,

whether the pressure drop increases or decreases when considering particle retention depends on which of these opposing effects is more dominant.

To better understand the effects of particle retention on the pressure drop profiles, we study separately:

1. The impact of suspended nanoparticles loss, by comparing a model without retention (i.e.,  $\lambda = 0$ ) with a model with retention but no permeability reduction, (i.e.,  $\theta_w = \theta_f = 0$ ).
2. The impact of suspended nanoparticles loss and permeability reduction, by comparing a model without retention with the complete model.

**Figure 12** presents the pressure drop profiles for the nanofluids without NaCl (NF1, NF3, and NF5). In the left panel of **Figure 12**, when only the loss of suspended nanoparticles is considered (solid lines), the pressure drop is lower compared to the case without retention (dashed lines). In the right panel of **Figure 12**, when permeability reduction is also taken into account (solid lines), the pressure drop is higher compared to the case without retention (dashed lines), particularly for NF5 (highest nanoparticle concentration). For the nanofluids with salt (NF2, NF4, and NF6), the results are similar, as shown in **Figure 13**. In this scenario, however, the loss of suspended nanoparticles due to retention is greater. Consequently, even when only this loss is considered, without accounting for permeability reduction, a significant difference in pressure drop for NF4 and NF6 is observed compared to the case without retention; see the left panel of **Figure 13**.



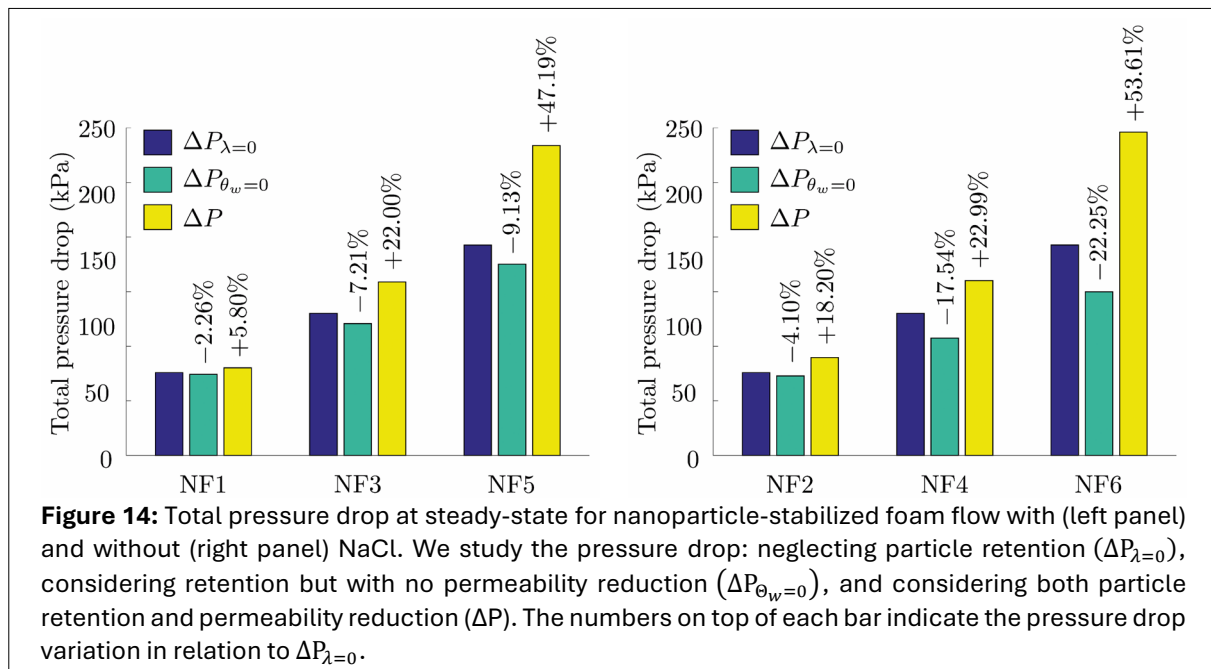
Let us quantify the difference in the pressure drop when retention is considered, compared to the case  $\lambda = 0$ . By substituting  $\sigma = \Gamma C$  from **Equation 32** into **Equation 37**, and after some calculations, the difference between the total pressure drop considering particle retention ( $\Delta P$ ) and the total pressure drop neglecting particle retention ( $\Delta P_{\lambda=0}$ ) can be written as (**Eq. 40**):

$$\Delta P - \Delta P_{\lambda=0} = \frac{u_w \mu_w}{k k_{rw}^0} \left[ \theta_w \Gamma \int_0^L \frac{C}{S^\beta} dx + \int_0^L \left( \frac{1}{S^\beta} - \frac{1}{S_{\lambda=0}^\beta} \right) dx \right]. \tag{40}$$

Analogously, the pressure drop considering retention but with no permeability reduction ( $\Delta P_{\theta_w=0}$ ) is given by (**Eq. 41**):

$$\Delta P_{\theta_w=0} - \Delta P_{\lambda=0} = \frac{u_w \mu_w}{k k_{rw}^0} \int_0^L \left( \frac{1}{S^\beta} - \frac{1}{S_{\lambda=0}^\beta} \right) dx. \tag{41}$$

**Figure 14** presents the total pressure drop for each nanofluid in the three cases. The numbers on top of each bar indicate the relative difference in pressure drop compared to the no-retention model.



Since the presence of NaCl is associated with higher ionic strength and, consequently, greater retention, we expect that neglecting particle retention will have a more pronounced effect in this case. Indeed, when there is no permeability reduction, the variation in pressure drop  $\Delta P_{\theta_w=0}$  relative to  $\Delta P_{\lambda=0}$  is smaller for NF1 compared to NF2, for NF3 compared to NF4, and for NF5 compared to NF6. All these differences are negative, indicating the dominance of nanoparticle loss decreasing the pressure drop. When permeability reduction is considered, neglecting particle retention also has a more pronounced effect for the case with NaCl. Nevertheless, the variation in pressure drop  $\Delta P$  relative to  $\Delta P_{\lambda=0}$  is positive, indicating the dominance of permeability reduction increasing the pressure drop.

Based on our findings, models that neglect nanoparticle retention and those that account for retention, but neglect permeability reduction underestimate the pressure drop. It is worth noting that, if we consider the complete model to be closer to reality, the model that considers only nanoparticle loss results in pressure drop values further from the actual behavior than the model that entirely neglects the retention phenomenon. The differences between these pressure drop estimates increase with the ionic strength and the nanoparticle concentration. Nevertheless, due to the lack of experimental data for higher concentrations, we employed the same retention parameters for NF5 and NF6 as those used for NF3 and NF4, respectively. Thus, further investigation is necessary to validate our results.

It is important to note that while higher pressure gradients can lead to increased water production, excessively high values may result in injectivity loss. Determining the optimal nanoparticle concentration that effectively stabilizes foam without causing detrimental retention during displacement is a key challenge for nanoparticle-stabilized foam, but advancing research in this field will rely on new experimental data. Conducting core-flooding experiments with foam flow poses significant challenges. Tracking the foam front as it moves through the medium requires advanced techniques like computed tomography or multiple high-precision pressure sensors, which makes these experiments both time-consuming and expensive. Analytical solutions can help predict flow behavior and optimize experimental design by providing estimates of maximum pressure drop and breakthrough time. This allows experiments to be planned with adequate pressure gauges and conducted for enough time to observe the expected flow behavior.

## 7. Conclusions

This study examined two-phase foam flow (water and gas) with suspended nanoparticles in the aqueous phase, incorporating the effects of particle retention and the resulting permeability reduction.

1. A semi-analytical solution was developed for nanoparticle-stabilized foam flow under steady-state conditions. In the absence of nanoparticles, the solution becomes analytic and is significantly simpler.
2. This solution allowed for the analysis of water saturation, foam apparent viscosity, and pressure drop profiles. Results were obtained for nanoparticle concentrations of 0.1, 0.5, and 1.0 wt%, both with and without NaCl, using retention parameters based on experimental data.
3. When comparing different nanoparticle concentrations, higher values lead to increased foam apparent viscosity, reducing steady-state water saturation and increasing pressure drop, thereby improving the sweep efficiency.
4. Comparing foam flows with and without nanoparticles, taking retention into account, resulted in enhanced sweep efficiency only for higher nanoparticle concentrations (0.5 and 1.0 wt%). For 0.1 wt% the difference is insignificant.
5. The semi-analytical steady-state solution showed excellent agreement when compared to a dynamic solution for foam flow with nanoparticles (neglecting particle retention).
6. When nanoparticle retention is considered, the loss of suspended nanoparticles diminishes their positive effect on foam's apparent viscosity, while the retained nanoparticles reduce permeability. These combined effects increase water saturation, generally leading to a lower pressure drop compared to models that ignore retention. Nevertheless, the reduction in permeability directly increases the pressure drop, so whether the pressure drop increases or decreases depends on which of these opposing effects is more dominant.
7. Based on our findings, models that neglect nanoparticle retention and those that account for retention but neglect permeability reduction underestimate the pressure drop. The differences between these pressure drop estimates increase in scenarios with significant retention (e.g., in the presence of NaCl and high nanoparticle concentration).

## STATEMENTS AND DECLARATIONS

### Acknowledgements

We thank Dr. Juliana Façanha for helpful discussions in improving the quality of this work. The authors gratefully acknowledge support from Shell Brasil through the project "Avançando na modelagem matemática e computacional para apoiar a implementação da tecnologia 'Foam-assisted WAG' em reservatórios do Pré-sal" [*Advancing mathematical and computational modeling to support the implementation of 'Foam-assisted WAG' technology in Pre-salt reservoirs*] (ANP 23518-4) at UFJF and the strategic importance of the support given by ANP through the R&D levy regulation. R.F. thanks Shell Global Solutions International from granting permission to publish this work. G.C. was partly supported by CNPq grants 306970/2022-8, 405366/2021-3, and FAPEMIG grant APQ-00206-24.

### Author Contributions

T. Danelon: Software, Methodology, Formal analysis, Investigation, Writing - Original Draft, Writing - Review & Editing. R. Farajzadeh: Conceptualization, Methodology, Formal analysis, Investigation, Supervision. P. Bedrikovetsky: Conceptualization, Methodology, Formal analysis, Investigation, Supervision. G. Chapiro: Conceptualization, Methodology, Formal analysis, Investigation, Writing - Review & Editing, Supervision, Project administration, Funding acquisition.

### Conflicts of Interest

The authors declare that they have no known competing financial interests or personal relationships that could have appeared to influence the work reported in this paper.

### Data, Code & Protocol Availability

No data, other than that described throughout the text, was used for the research described in the article. Software used to solve the equations is not being publicly shared.

## ORCID IDs

Tatiana Danelon  <https://orcid.org/0000-0003-0198-936X>  
 Rouhi Farajzadeh  <https://orcid.org/0000-0003-3497-0526>  
 Pavel Bedrikovetsky  <https://orcid.org/0000-0002-4786-8275>  
 Grigori Chapiro  <https://orcid.org/0000-0003-4568-834X>

### Correction from May 5, 2025:

Please note that Figure 14 was not showing in the original pdf. This issue has now been corrected, and the pdf has been updated online.

## REFERENCES

1. Arain, Z.-U.-A., Al-Ansari, S., Ali, M., Memon, S., Bhatti, M. A., Lagat, C., & Sarmadivaleh, M. (2020). Reversible and irreversible adsorption of bare and hybrid silica nanoparticles onto carbonate surface at reservoir condition. *Petroleum*, 6(3), 277–285. <https://doi.org/10.1016/j.petlm.2019.09.001>
2. Ashoori, E., Marchesin, D., & Rossen, W. R. (2011). Roles of transient and local equilibrium foam behavior in porous media: Traveling wave. *Colloids and Surfaces A: Physicochemical and Engineering Aspects*, 377(1–3), 228–242. <https://doi.org/10.1016/j.colsurfa.2010.12.042>
3. Babakhani, P., Bridge, J., Doong, R., & Phenrat, T. (2017). Continuum-based models and concepts for the transport of nanoparticles in saturated porous media: A state-of-the-science review. *Advances in Colloid and Interface Science*, 246, 75–104. <https://doi.org/10.1016/j.cis.2017.06.002>
4. Bedrikovetsky, P. (2013). *Mathematical theory of oil and gas recovery: with applications to ex-USSR oil and gas fields* (Vol. 4). Springer Science & Business Media.
5. Bedrikovetsky, P., Marchesin, D., Shecaira, F., Souza, A. L., Milanez, P. V., & Rezende, E. (2001). Characterisation of deep bed filtration system from laboratory pressure drop measurements. *Journal of Petroleum Science and Engineering*, 32(2–4), 167–177. [https://doi.org/10.1016/S0920-4105\(01\)00159-0](https://doi.org/10.1016/S0920-4105(01)00159-0)
6. Bennetzen, M. V., & Mogensen, K. (2014). Novel applications of nanoparticles for future enhanced oil recovery. *All Days*, IPTC-17857-MS. <https://doi.org/10.2523/IPTC-17857-MS>
7. Borazjani, S., Dehdari, L., & Bedrikovetsky, P. (2020). Exact solution for tertiary polymer flooding with polymer mechanical entrapment and adsorption. *Transport in Porous Media*, 134(1), 41–75. <https://doi.org/10.1007/s11242-020-01436-7>
8. Collins, R. E. (1976). *Flow of fluids through porous materials*. Petroleum Publishing, Tulsa, OK. OSTI ID:7099752
9. Danelon, T., Paz, P., & Chapiro, G. (2024a). The mathematical model and analysis of the nanoparticle-stabilized foam displacement. *Applied Mathematical Modelling*, 125, 630–649. <https://doi.org/10.1016/j.apm.2023.10.022>
10. Danelon, T., Rocha, B. M., Dos Santos, R. W., & Chapiro, G. (2024b). Sensitivity analysis and uncertainty quantification based on the analytical solution for nanoparticle-stabilized foam flow in porous media. *Geoenergy Science and Engineering*, 242, 213285. <https://doi.org/10.1016/j.geoen.2024.213285>
11. Daneshfar, R., Ashoori, S., & Soltani Soulgani, B. (2024). Transport and retention of silica nanoparticles in glass-bead columns: Effects of particle size, type, and concentration of ionic species. *Scientific Reports*, 14(1), 685. <https://doi.org/10.1038/s41598-023-51119-8>
12. Daryasafar, A., & Shahbazi, K. (2018). Using nanotechnology for CO<sub>2</sub>-foams stabilization for application in enhanced oil recovery. *International Journal of Energy for a Clean Environment*, 19(3–4), 217–235. <https://doi.org/10.1615/InterJenerCleanEnv.2018026111>
13. Du, D., Zhao, D., Li, Y., Wang, F., & Li, J. (2021). Parameter calibration of the stochastic bubble population balance model for predicting NP-stabilized foam flow characteristics in porous media. *Colloids and Surfaces A: Physicochemical and Engineering Aspects*, 614, 126180. <https://doi.org/10.1016/j.colsurfa.2021.126180>
14. Eftekhari, A. A., & Farajzadeh, R. (2017). Effect of foam on liquid phase mobility in porous media. *Scientific Reports*, 7(1), 43870. <https://doi.org/10.1038/srep43870>
15. Eide, Ø., Fernø, M., Bryant, S., Kovscek, A., & Gautepllass, J. (2020). Population-balance modeling of CO<sub>2</sub> foam for CCUS using nanoparticles. *Journal of Natural Gas Science and Engineering*, 80, 103378. <https://doi.org/10.1016/j.jngse.2020.103378>

16. Espinosa, D., Caldelas, F., Johnston, K., Bryant, S. L., & Huh, C. (2010). Nanoparticle-stabilized supercritical CO<sub>2</sub> foams for potential mobility control applications. *SPE Improved Oil Recovery Symposium*, SPE-129925-MS. <https://doi.org/10.2118/129925-MS>
17. Façanha, J. M. F., Lopes, L. F., Fritis, G., Godoy, P., Weber Dos Santos, R., Chapiro, G., & Perez-Gramatges, A. (2022). Bubble-growth regime for confined foams: Comparison between N<sub>2</sub>-CO<sub>2</sub>/foam and CO<sub>2</sub>/foam stabilized by silica nanoparticles. *Journal of Petroleum Science and Engineering*, 218, 111006. <https://doi.org/10.1016/j.petrol.2022.111006>
18. Fadili, A., Murtaza, A., & Zitha, P. (2022). Injectivity decline by nanoparticles transport in high permeable rock. *Journal of Petroleum Science and Engineering*, 211, 110121. <https://doi.org/10.1016/j.petrol.2022.110121>
19. Farajzadeh, R., Bedrikovetsky, P., Lotfollahi, M., & Lake, L. W. (2016). Simultaneous sorption and mechanical entrapment during polymer flow through porous media. *Water Resources Research*, 52(3), 2279–2298. <https://doi.org/10.1002/2015WR017885>
20. Hajjabad, S. H., Bedrikovetsky, P., Mahani, H., Khoshsima, A., Aghaei, H., Kalateh-Aghamohammadi, M., & Habibi, S. (2020). Effects of surface modified nanosilica on drilling fluid and formation damage. *Journal of Petroleum Science and Engineering*, 194, 107559. <https://doi.org/10.1016/j.petrol.2020.107559>
21. Herzig, J. P., Leclerc, D. M., & Goff, P. Le. (1970). Flow of suspensions through porous media—Application to deep filtration. *Industrial & Engineering Chemistry*, 62(5), 8–35. <https://doi.org/10.1021/ie50725a003>
22. Hirasaki, G. J., & Lawson, J. B. (1985). Mechanisms of foam flow in porous media: apparent viscosity in smooth capillaries. *Society of Petroleum Engineers Journal*, 25(02), 176–190. <https://doi.org/10.2118/12129-PA>
23. Issakhov, M., Khanjani, M., Muratkhozhina, A., Pourafshary, P., Aidarova, S., & Sharipova, A. (2024). Experimental and data-driven analysis for predicting nanofluid performance in improving foam stability and reducing mobility at critical micelle concentration. *Scientific Reports*, 14(1), 7856. <https://doi.org/10.1038/s41598-024-58609-3>
24. Kam, S. I. (2008). Improved mechanistic foam simulation with foam catastrophe theory. *Colloids and Surfaces A: Physicochemical and Engineering Aspects*, 318(1–3), 62–77. <https://doi.org/10.1016/j.colsurfa.2007.12.017>
25. Keykhosravi, A., Bedrikovetsky, P., & Simjoo, M. (2022). Experimental insight into the silica nanoparticle transport in dolomite rocks: Spotlight on DLVO theory and permeability impairment. *Journal of Petroleum Science and Engineering*, 209, 109830. <https://doi.org/10.1016/j.petrol.2021.109830>
26. Kavscek, A. R., Patzek, T. W., & Radke, C. J. (1995). A mechanistic population balance model for transient and steady-state foam flow in Boise sandstone. *Chemical Engineering Science*, 50(23), 3783–3799. [https://doi.org/10.1016/0009-2509\(95\)00199-F](https://doi.org/10.1016/0009-2509(95)00199-F)
27. Li, Q., & Prigiobbe, V. (2020). Modeling nanoparticle transport in porous media in the presence of a foam. *Transport in Porous Media*, 131(1), 269–288. <https://doi.org/10.1007/s11242-019-01235-9>
28. Li, S., Li, Z., & Wang, P. (2016). Experimental study of the stabilization of CO<sub>2</sub> foam by sodium dodecyl sulfate and hydrophobic nanoparticles. *Industrial & Engineering Chemistry Research*, 55(5), 1243–1253. <https://doi.org/10.1021/acs.iecr.5b04443>
29. Li, Y., Wang, Y., Pennell, K. D., & Abriola, L. M. (2008). Investigation of the transport and deposition of fullerene (C<sub>60</sub>) nanoparticles in quartz sands under varying flow conditions. *Environmental Science & Technology*, 42(19), 7174–7180. <https://doi.org/10.1021/es801305y>
30. Rahman, A., Torabi, F., & Shirif, E. (2023). Surfactant and nanoparticle synergy: Towards improved foam stability. *Petroleum*, 9(2), 255–264. <https://doi.org/10.1016/j.petlm.2023.02.002>
31. Rodriguez, E., Roberts, M. R., Yu, H., Huh, C., & Bryant, S. L. (2009). Enhanced migration of surface-treated nanoparticles in sedimentary rocks. *SPE Annual Technical Conference and Exhibition*, SPE-124418-MS. <https://doi.org/10.2118/124418-MS>
32. Roebroeks, J., Eftekhari, A. A., Farajzadeh, R., & Vincent-Bonnieu, S. (2015, April 14). Nanoparticle stabilized foam in carbonate and sandstone reservoirs. *IOR 2015 - 18th European Symposium on Improved Oil Recovery, Dresden, Germany*. <https://doi.org/10.3997/2214-4609.201412121>
33. Rognmo, A. U., Horjen, H., & Fernø, M. A. (2017). Nanotechnology for improved CO<sub>2</sub> utilization in CCS: Laboratory study of CO<sub>2</sub>-foam flow and silica nanoparticle retention in porous media. *International Journal of Greenhouse Gas Control*, 64, 113–118. <https://doi.org/10.1016/j.ijggc.2017.07.010>
34. Rognmo, A. U., Al-Khayyat, N., Heldal, S., Vikingstad, I., Eide, Ø., et al (2020). Performance of silica nanoparticles in CO<sub>2</sub> foam for EOR and CCUS at tough reservoir conditions. *SPE Journal*, 25(01), 406–415. <https://doi.org/10.2118/191318-PA>
35. Sameni, A., Pourafshary, P., Ghanbarzadeh, M., & Ayatollahi, S. (2015). Effect of nanoparticles on clay swelling and migration. *Egyptian Journal of Petroleum*, 24(4), 429–437. <https://doi.org/10.1016/j.ejpe.2015.10.006>
36. Sharma, M. M., & Yortsos, Y. C. (1987). Transport of particulate suspensions in porous media: Model formulation. *AIChE Journal*, 33(10), 1636–1643. <https://doi.org/10.1002/aic.690331007>
37. Simjoo, M., Dong, Y., Andrianov, A., Talanana, M., & Zitha, P. L. J. (2013). Novel insight into foam mobility control. *SPE Journal*, 18(03), 416–427. <https://doi.org/10.2118/163092-PA>

38. Simjoo, M., & Zitha, P. L. J. (2015). Modeling of foam flow using stochastic bubble population model and experimental validation. *Transport in Porous Media*, 107(3), 799–820. <https://doi.org/10.1007/s11242-015-0468-y>
39. Singh, R., & Mohanty, K. K. (2015). Synergy between nanoparticles and surfactants in stabilizing foams for oil recovery. *Energy & Fuels*, 29(2), 467–479. <https://doi.org/10.1021/ef5015007>
40. Sun, Q., Li, Z., Li, S., Jiang, L., Wang, J., & Wang, P. (2014). Utilization of surfactant-stabilized foam for enhanced oil recovery by adding nanoparticles. *Energy & Fuels*, 28(4), 2384–2394. <https://doi.org/10.1021/ef402453b>
41. Sun, Q., Liu, W., Li, S., Zhang, N., & Li, Z. (2021). Interfacial rheology of foam stabilized by nanoparticles and their retention in porous media. *Energy & Fuels*, 35(8), 6541–6552. <https://doi.org/10.1021/acs.energyfuels.0c03680>
42. Tang, J., Castañeda, P., Marchesin, D., & Rossen, W. R. (2019). Three-phase fractional-flow theory of foam-oil displacement in porous media with multiple steady states. *Water Resources Research*, 55(12), 10319–10339. <https://doi.org/10.1029/2019WR025264>
43. Tufenkji, N., & Elimelech, M. (2004). Deviation from the classical colloid filtration theory in the presence of repulsive DLVO interactions. *Langmuir*, 20(25), 10818–10828. <https://doi.org/10.1021/la0486638>
44. Wang, Y., Li, Y., Fortner, J. D., Hughes, J. B., Abriola, L. M., & Pennell, K. D. (2008). Transport and retention of nanoscale c60 aggregates in water-saturated porous media. *Environmental Science & Technology*, 42(10), 3588–3594. <https://doi.org/10.1021/es800128m>
45. Yekeen, N., Idris, A. K., Manan, M. A., Samin, A. M., Risal, A. R., & Kun, T. X. (2017). Bulk and bubble-scale experimental studies of influence of nanoparticles on foam stability. *Chinese Journal of Chemical Engineering*, 25(3), 347–357. <https://doi.org/10.1016/j.cjche.2016.08.012>
46. Yekeen, N., Manan, M. A., Idris, A. K., Padmanabhan, E., Junin, R., Samin, A. M., Gbadamosi, A. O., & Oguamah, I. (2018). A comprehensive review of experimental studies of nanoparticles-stabilized foam for enhanced oil recovery. *Journal of Petroleum Science and Engineering*, 164, 43–74. <https://doi.org/10.1016/j.petrol.2018.01.035>
47. Yu, H., Kotsmar, C., Yoon, K. Y., Ingram, D. R., Johnston, K. P., Bryant, S. L., & Huh, C. (2010). Transport and retention of aqueous dispersions of paramagnetic nanoparticles in reservoir rocks. *SPE Improved Oil Recovery Symposium*, SPE-129887-MS. <https://doi.org/10.2118/129887-MS>
48. Zavala, R. Q., Lozano, L. F., Zitha, P. L. J., & Chapiro, G. (2022). Analytical solution for the population-balance model describing foam displacement. *Transport in Porous Media*, 144(1), 211–227. <https://doi.org/10.1007/s11242-021-01589-z>
49. Zeinijahromi, A., Farajzadeh, R., (Hans) Bruining, J., & Bedrikovetsky, P. (2016). Effect of fines migration on oil-water relative permeability during two-phase flow in porous media. *Fuel*, 176, 222–236. <https://doi.org/10.1016/j.fuel.2016.02.066>
50. Zhang, T. (2012). Modeling of nanoparticle transport in porous media. PhD thesis, The University of Texas at Austin. <http://hdl.handle.net/2152/ETD-UT-2012-08-6044>
51. Zhang, T., Murphy, M., Yu, H., Huh, C., & Bryant, S. L. (2016). Mechanistic model for nanoparticle retention in porous media. *Transport in Porous Media*, 115(2), 387–406. <https://doi.org/10.1007/s11242-016-0711-1>
52. Zhang, T., Murphy, M. J., Yu, H., Bagaria, H. G., Yoon, K. Y., Neilson, B. M., Bielawski, C. W., Johnston, K. P., Huh, C., & Bryant, S. L. (2015). Investigation of nanoparticle adsorption during transport in porous media. *SPE Journal*, 20(04), 667–677. <https://doi.org/10.2118/166346-PA>
53. Zitha, P. L. J., & Du, D. X. (2010). A new stochastic bubble population model for foam flow in porous media. *Transport in Porous Media*, 83(3), 603–621. <https://doi.org/10.1007/s11242-009-9462-6>